

Imidazole Based Ruthenium(IV) Complexes as Highly Efficient Bifunctional Catalysts for the Redox Isomerization of Allylic Alcohols in Aqueous Medium: Water as Cooperating Ligand

Josefina Díez,[†] José Gimeno,^{*,†} Agustí Lledós,^{*,‡} Francisco J. Suárez,[†] and Cristian Vicent[§]

[†]Laboratorio de Química Organometálica y Catálisis (Unidad Asociada al C.S.I.C.), Departamento de Química Orgánica e Inorgánica, Instituto Universitario de Química Organometálica "Enrique Moles", Universidad de Oviedo, 33071 Oviedo, Spain

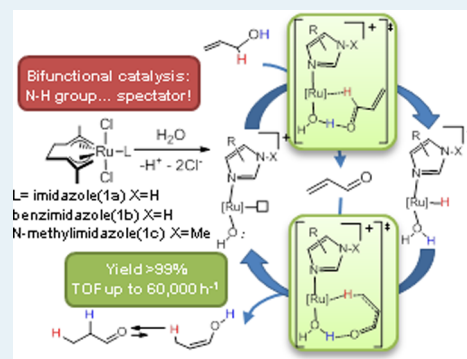
[‡]Departament de Química, Universitat Autònoma de Barcelona, Cerdanyola del Vallès, 08193, Barcelona, Spain

[§]Serveis Centrals d'Instrumentació Científica, Universitat Jaume I, Avenida Sos Baynat s/n, 12071 Castelló, Spain

Supporting Information

ABSTRACT: Bis-allyl ruthenium(IV) complexes containing 1,3 azole β -N-H protic ligands $[\text{Ru}(\eta^3\text{-}\eta^3\text{-C}_{10}\text{H}_{16})\text{Cl}_2\text{L}]$ ($\text{C}_{10}\text{H}_{16}$ = 2,7-dimethylocta-2,6-diene-1,8-diyl) (L = imidazole (1a), benzimidazole (1b)), and N-methylimidazole (1c) are highly active precatalysts in the redox isomerization of allylic alcohols into carbonyl compounds in aqueous medium and in the absence of base. A wide series of primary and secondary allylic alcohols can be isomerized into the corresponding carbonyl compounds. Remarkably, complex 1b has been found to be the most efficient catalyst reported to date for the isomerization of 1-octen-3-ol in water leading to a turnover frequency (TOF) value of 60 000 h^{-1} . Moreover, catalyst 1b can be recycled remaining active up to seven cycles. Density functional theory (DFT) calculations give evidence that the hydroxo complexes derived from 1a–c species can be formed in aqueous solution and that they can act as the catalytic active species in a bifunctional catalyzed process. This study demonstrate that in water the participation of the β -N-H protic group of the 1,3-azole ligands in the bifunctional catalysis is not required, provided that a water molecule can act as cooperating ligand.

KEYWORDS: allylic alcohols, aqueous medium, cooperating ligands, DFT calculations, redox isomerization, ruthenium catalysts

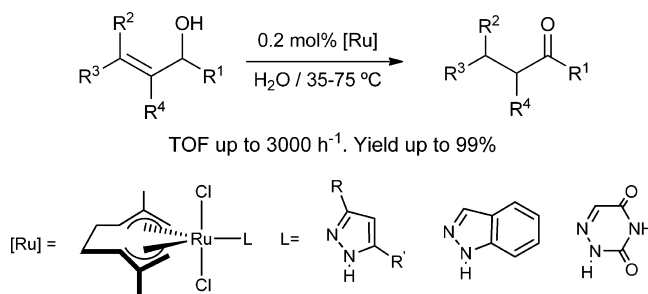


INTRODUCTION

Transition metal catalyzed isomerization of allylic alcohols has become a very useful synthetic methodology of carbonyl derivatives, much more attractive than those procedures based on classic stoichiometric reactions which involve a two-step sequential oxidation and reduction processes using highly reactive reagents. During the past decade a large number of highly efficient synthetic routes have been reported disclosing genuine examples of atom economy processes with both academic and industrial interest.^{1–5} Among the most striking developments, catalytic systems working in aqueous medium are particularly relevant especially those using water as unique solvent since they are able to perform more efficient transformations vs those using organic solvents.^{6–23}

During the past few years, our research group has been engaged in the development of redox isomerization of allylic alcohols in aqueous medium catalyzed by ruthenium(II) and ruthenium(IV) complexes which proceed in excellent yields under mild reaction conditions.^{3,24–38} More recently, we have reported that ruthenium(IV) complexes $[\text{Ru}(\eta^3\text{-}\eta^3\text{-C}_{10}\text{H}_{16})\text{Cl}_2(\text{L})]$ containing pyrazole based and other analogous ligands containing α -N-H protic groups (see Chart 1) are highly active catalysts in water including the transformation at 35 °C and in the absence of base.^{39,40}

Chart 1



It has been shown (by Electrospray Ionization Mass Spectrometry (ESI-MS)) that aqua-complexes of the type $[\text{Ru}(\eta^3\text{-}\eta^3\text{-C}_{10}\text{H}_{16})\text{Cl}(\text{H}_2\text{O})(\text{pyrazole})]^+$ (A) and $[\text{Ru}(\eta^3\text{-}\eta^3\text{-C}_{10}\text{H}_{16})(\text{H}_2\text{O})(\text{OH})(\text{pyrazole})]^+$ (B) (see Chart 2) are formed in solution and play an important role on the catalytic activity.⁴⁰

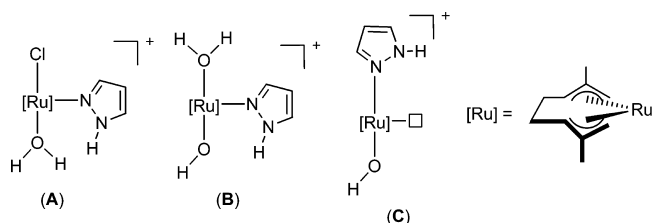
Remarkably, theoretical studies (density functional theory (DFT)) reveal that hydroxo species (B and C) generated by

Received: June 11, 2012

Revised: August 22, 2012

Published: August 27, 2012

Chart 2

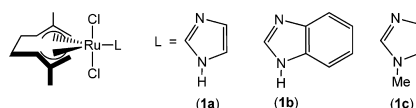


deprotonation of the corresponding aqua-complexes are acting as metal–ligand bifunctional catalysts, disclosing concerted outer-sphere mechanisms via transition states [TS1] and [TS2], which favor overall lower energy barriers (Scheme 1). The isomerization implies two hydrogen-transfer steps from the substrate to the catalyst and subsequent transfer back to the substrate. Motivated by these findings we wondered whether other 1,3-azole β -N-H protic heterocycles, that is, imidazole derivatives, might also provide cooperative effects based on analogous ligand–substrate hydrogen interactions enabling alternative favored outer-sphere mechanisms. In these derivatives there is no accessible NH site able to take part in Noyori-type metal–ligand bifunctional catalysis.

Herein, we describe that bis-allyl ruthenium(IV) complexes $[\text{Ru}(\eta^3:\eta^3\text{-C}_{10}\text{H}_{16})\text{Cl}_2(\text{L})]$ (L = imidazole (**1a**), benzimidazole (**1b**)) (Chart 3) are also highly efficient catalysts for the isomerization of allylic alcohols into carbonyl compounds in aqueous media and in the absence of base. In particular, the following remarkable novel features have been found by using these catalysts: (i) the efficiency of catalyst **1b** is much higher than that shown by analogous pyrazole partner (TOF = 60000 vs 3000 h^{-1}) which, as far as we know, is the most efficient catalyst described to date in water and in the absence of base; (ii) it is active at room temperature; (iii) ESI mass spectra reveal the existence of dissociation processes and the presence of cationic aqua-complexes analogous to **A** and **B** which are the actual active catalytic species.

On the basis of these experimental results the catalytic mechanism has been analyzed theoretically. Different competitive pathways reveal outer-sphere mechanisms enabled by the formation of aqua-complexes and their deprotonated species. The most remarkable feature relies on the fact that the uncoordinated N-H group of imidazole remains unchanged acting as a spectator ligand during the whole catalytic cycle. This fact seems to suggest that the use of *N*-substituted 1,3-azole ligands should also give rise to active catalytic species. Experimental confirmation of this theoretical prediction was obtained by studying the catalytic activity of the complex $[\text{Ru}(\eta^3:\eta^3\text{-C}_{10}\text{H}_{16})\text{Cl}_2(\text{L})]$ (L = *N*-methylimidazole) (**1c**) in water. In marked contrast to the usual behavior of Noyori

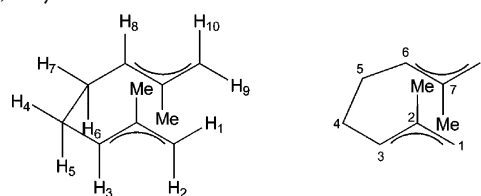
Chart 3



catalysts, which lost any activity when the key NH sites are methylated,⁴¹ **1c** shows a remarkable catalytic activity in water.

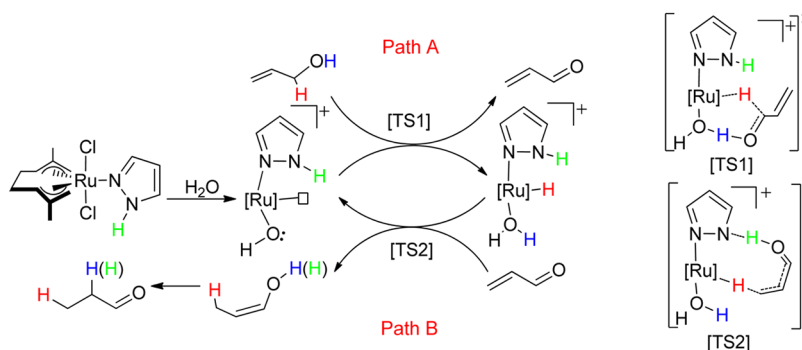
EXPERIMENTAL SECTION

The manipulations were performed under an atmosphere of dry nitrogen using vacuum-line and standard Schlenk techniques. Solvents were dried by standard methods and distilled under nitrogen before use. All reagents were from suppliers and used without further purification with the exception of compounds $[\{\text{Ru}(\eta^3:\eta^3\text{-C}_{10}\text{H}_{16})(\mu\text{-Cl})\text{Cl}_2\}]$ (**1**),^{42–44} $[\{\text{Ru}(\eta^6\text{-arene})(\mu\text{-Cl})\text{Cl}_2\}]$ (arene = C_6H_6 , *p*-cymene, C_6Me_6),^{45,46} $[\text{Ru}(\eta^6\text{-p-cymene})\text{Cl}_2(\text{benzimidazole})]$ (**2b**)^{47,48} (conductivity in water, 20 °C: $173 \Omega^{-1} \text{cm}^2 \text{mol}^{-1}$), $[\text{Ru}(\eta^6\text{-C}_6\text{Me}_6)\text{Cl}_2(\text{benzimidazole})]$ (**2c**)^{46,47} (conductivity in water, 20 °C: $180 \Omega^{-1} \text{cm}^2 \text{mol}^{-1}$), which were prepared by following the methods reported in the literature. Infrared spectra were recorded on a Perkin-Elmer 1720-XFT spectrometer. The conductivities were measured at room temperature, in about $10^{-3} \text{mol dm}^{-3}$ water solutions, with a Jenway PCM3 conductimeter. pH measurements have been performed with a WTW Microprocessor pH-meter with a SenTix50T electrode. The C and H analyses were carried out with a Perkin-Elmer 2400 micro-analyzer. GC measurements were made on Hewlett-Packard HP6890 equipment using a HP-INNOWAX cross-linked poly(ethyleneglycol) (30 m, 250 μm) or a Supelco Beta-Dex 120 (30 m, 250 μm) column. GC/MS measurements were performed on Agilent 6890N equipment coupled to a 5973 mass detector (70 eV electron impact ionization) using a HP-1MS column. NMR spectra were recorded on a Bruker DPX-300 instrument at 300 MHz (¹H) or 75.4 MHz (¹³C) using SiMe₄ as standard. DEPT experiments have been carried out for all of the compounds reported. The numbering for protons and carbons of the 2,7-dimethylocta-2,6-diene-1,8-diyl skeleton is as follows:



Electrospray Ionization Mass Spectrometry. A Quattro LC (QhQ quadrupole–hexapole–quadrupole) mass spectrometer

Scheme 1. Mechanism of the Isomerization of Allylic Alcohols Catalyzed by Pyrazole-Based Ruthenium(IV) Complexes in Water⁴⁰



with an orthogonal Z-spray-electrospray interface (Waters, Manchester, U.K.) was used. The drying gas as well as nebulizing gas was nitrogen at a flow of 300 and 50 L/h, respectively. The temperature of the source block was set to 100 °C and the interface to 120 °C. The capillary voltage was set at 3.5 kV in the positive scan mode, and the cone voltage was adjusted to a low value (typically $U_c = 5-15$ V) to control the extent of fragmentation in the source region. Sample solutions (ca. 5×10^{-4} M) in the appropriate solvent were introduced through a fused-silica capillary to the ESI source via syringe pump at a flow rate of 10 μ L/min. The chemical composition of each peak obtained in the full scan mode was assigned by comparison of the isotope experimental and theoretical patterns using the MassLynx 4.0 program. Collision induced dissociation (CID) experiments were performed with argon at various collision energies, ranging from $E_{lab} = 3-15$ eV. The most intense precursor peak of interest was mass-selected with Q1 (isolation width of 1 Da), interacted with argon in the hexapole cell while scanning Q2 to monitor the ionic fragments. Typically, water speciation of compounds **1a-1c** was investigated in triplicate where reproducibility was observed. The temporal evolution of the ESI mass spectra of compounds **1a-1c** in water was investigated at different time intervals encompassing $t = 0$ h to $t = 1$ h.

Synthesis of [Ru(η^3 - η^3 -C₁₀H₁₆)Cl₂(L)] (L = imidazole (1a**), benzimidazole (**1b**), *N*-methylimidazole (**1c**)).** A stoichiometric amount of 1,3-azole (0.64 mmol) was added, at room temperature, to a solution of complex [$\{Ru(\eta^3$ - η^3 -C₁₀H₁₆)-(μ -Cl)Cl₂}] (**1**) (0.200 g; 0.32 mmol) in 20 mL of dichloromethane. After the mixture was stirred for 10 min, the solvent was removed under vacuum, and the resulting orange solid residue was washed with hexane (3 \times 10 mL) and dried in vacuo. **1a**: Yield 63% (0.152 g). Anal. Calcd for RuC₁₃H₂₀N₂Cl₂: C, 41.49; H, 5.36; N, 7.44. Found: C (41.40), H (4.49), N (7.56). IR (KBr, cm⁻¹): ν 611 (s), 653 (s), 753 (s), 952 (m), 1023 (m), 1060 (vs), 1100 (m), 1319 (m), 1380 (m), 1455 (m), 1540 (m), 2916 (m), 3143 (m), 3270 (s). ¹H NMR (CD₂Cl₂): δ 2.33 (s, 6H, 2xCH₃), 2.42 (m, 2H, H₄ and H₆), 3.06 (m, 2H, H₅ and H₇), 4.31 (s, 2H, H₂ and H₁₀), 4.47 (s, 2H, H₁ and H₉), 5.11 (m, 2H, H₃ and H₈), 7.09 (s, 1H, H₅ L), 7.64 (s, 1H, H₄ L), 8.29 (s, 1H, H₂ L), 9.70 (s, 1H, NH) ppm. ¹³C{¹H} NMR (CD₂Cl₂): δ 20.8 (s, 2xCH₃), 36.4 (s, C₄ and C₅), 77.6 (s, C₁ and C₈), 94.9 (s, C₃ and C₆), 115.7 (s, C₅ L), 129.1 (s, C₂ and C₇), 130.8 (s, C₄ L), 139.3 (s, C₂ L) ppm. Conductivity (water, 20 °C): 108 Ω^{-1} cm² mol⁻¹. **1b**: Yield 76% (0.210 g). Anal. Calcd for RuC₁₇H₂₂N₂Cl₂: C, 47.89; H, 5.20; N, 6.57. Found: C, 47.93; H, 5.17; N, 6.63. IR (KBr, cm⁻¹): ν 613 (w), 701 (w), 750 (vs), 763 (w), 887 (w), 962 (m), 1012 (m), 1031 (m), 1111 (m), 1151 (m), 1248 (m), 1261 (m), 1302 (m), 1361 (m), 1383 (m), 1418 (s), 1456 (m), 1494 (m), 1618 (w), 2907 (m), 3136 (s), 3197 (s). ¹H NMR (*d*⁸-THF): δ 2.42 (m, 2H, H₄ and H₆), 2.49 (s, 6H, 2xCH₃), 3.11 (m, 2H, H₅ and H₇), 4.54 (s, 2H, H₂ and H₁₀), 4.97 (s, 2H, H₁ and H₉), 5.22 (m, 2H, H₃ and H₈), 7.30-7.40 (m, 2H, H₆ and H₇ L), 7.56 (d, 1H, $J_{HH} = 8.4$ Hz, H₈ L), 8.48 (d, 1H, $J_{HH} = 8.1$ Hz, H₅ L), 8.86 (s, 1H, H₂ L), 9.71 (s, 1H, NH) (s, 1H, NH) ppm. ¹³C{¹H} NMR (*d*⁸-THF): δ 21.4 (s, 2xCH₃), 37.0 (s, C₄ and C₅), 78.2 (s, C₁ and C₈), 95.4 (s, C₃ and C₆), 103.3 (s, C₉ L), 112.7 (s, C₅ L), 122.6 (s, C₆ L), 123.3 (s, C₇ L), 123.8 (s, C₈ L), 129.7 (s, C₂ and C₇), 134.7 (s, C₄ L), 148.9 (s, C₂ L) ppm. **1c**: Yield 72% (0.180 g). Anal. Calcd for RuC₁₃H₂₀N₂Cl₂: C, 43.08; H, 5.68; N, 7.18. Found: C, 43.27; H, 5.85; N, 7.25. IR (KBr, cm⁻¹): ν 619 (m), 658 (m), 753 (f), 861 (m), 1023 (m), 1093 (mf), 1110 (f), 1238 (m), 1379 (m), 1423 (m), 1456 (m), 1536 (m), 2916 (m), 3118 (f). ¹H NMR

(CD₂Cl₂): δ 2.36 (s, 6H, 2xCH₃), 2.41 (m, 2H, H₄ and H₆), 3.03 (m, 2H, H₅ and H₇), 3.71 (s, 3H, N-CH₃), 4.28 (s, 2H, H₂ and H₁₀), 4.45 (s, 2H, H₁ and H₉), 5.09 (m, 2H, H₃ and H₈), 6.64 (s, 1H, H₅ L), 7.56 (s, 1H, H₄ L), 8.11 (s, 1H, H₂ L) ppm. ¹³C{¹H} NMR (CD₂Cl₂): δ 20.8 (s, 2xCH₃), 34.5 (s, N-CH₃), 36.4 (s, C₄ and C₅), 77.6 (s, C₁ and C₈), 94.7 (s, C₃ and C₆), 120.2 (s, C₅ L), 128.9 (s, C₂ and C₇), 131.6 (s, C₄ L), 141.5 (s, C₂ L) ppm. Conductivity (water, 20 °C): 75 Ω^{-1} cm² mol⁻¹.

Synthesis of Complex [RuCl₂(η^6 -C₆H₆)(benzimidazole)] (2a**).** A mixture of [$\{RuCl(\mu$ -Cl)(η^6 -C₆H₆)₂] (250 mg, 0.5 mmol) and benzimidazole (1 mmol) in methanol (20 mL) was stirred for 1 h. Then the solvent was removed under vacuum, and the resulting orange solid residue was recrystallized in dichloromethane/diethylether and dried in vacuo. Yield 76% (279 mg). Anal. Calcd for RuC₁₃H₁₂N₂Cl₂: C, 42.40; H, 3.28; N, 7.61. Found: C, 42.55; H, 3.32; N, 7.57. IR (KBr, cm⁻¹): 618 (w), 744 (vs), 775 (w), 844 (s), 879 (w), 977 (w), 1006 (m), 1108 (w), 1140 (w), 1195 (w), 1247 (s), 1269 (m), 1305 (m), 1408 (s), 1432 (s), 1458 (m), 1485 (m), 1496 (w), 1595 (w), 3062 (m), 3125 (m), 3164 (vs), 3434 (s). ¹H NMR (CDCl₃): δ 5.76 (s, 6H, C₆H₆), 7.10-7.70 (m, 4H, H₄, H₅, H₆, H₇ L), 8.37 (s, 1H, H₂ L), 9.16 (s, 1H, NH) ppm. Conductivity (water, 20 °C): 190 Ω^{-1} cm² mol⁻¹.

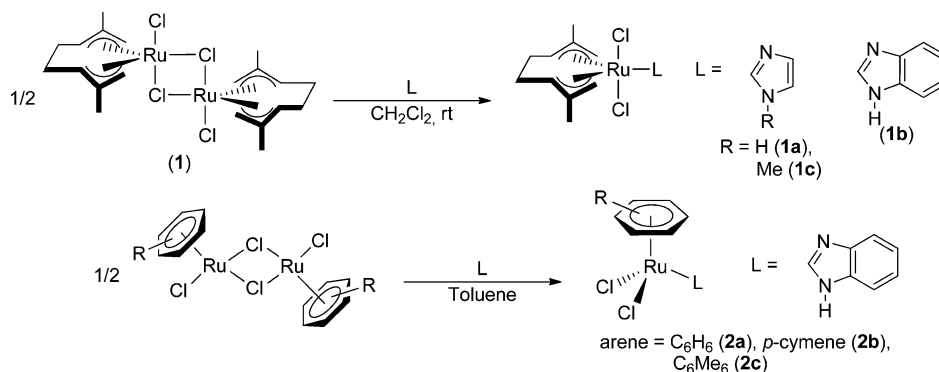
General Procedure for the Catalytic Isomerization of Allylic Alcohols into Carbonyl Compounds. In a sealed tube 4 mmol of the corresponding allylic alcohol, the ruthenium catalyst precursor, and cocatalyst (if required) were dissolved in tetrahydrofuran (THF) or water (20 mL), and the reaction mixture was stirred at 75 °C for the indicated time. The course of the reaction was monitored by regular sampling and analysis by gas chromatography every five minutes. Only turnover frequency (TOF) values at quantitative transformations are reported (otherwise, it is indicated properly). The identity of the resulting saturated carbonyl compounds was assessed by comparison with commercially available pure samples (Aldrich Chemical Co. or Acros Organics) and by their fragmentation in GC/MS. Catalyst recycling is carried out by liquid-liquid extraction of the product with diethyl ether (3 \times 5 mL) and subsequent addition of substrate.

X-ray Crystal Structure Determination of Complexes **1a, **1b**, and **1c**.** Crystals suitable for X-ray diffraction analysis were obtained, for **1a** and **1c**, by slow diffusion of hexane into a saturated solution of the complexes in dichloromethane, and for **1b**, were obtained from tetrahydrofuran/diethylether solvent system. The most relevant crystal and refinement data are collected in the Supporting Information, Table S1.

For **1a** and **1c**, diffraction data were recorded on a Nonius KappaCCD single crystal diffractometer, using Mo- $K\alpha$ radiation ($\alpha = 0.71073$ Å). In both cases images were collected at a 35 mm fixed crystal-detector distance, using the oscillation method, with 1° oscillation and 50 s exposure time per frame. Data collection strategy was calculated with the program Collect.⁴⁹ Data reduction and cell refinement were performed with the programs HKL Denzo and Scalepack.⁵⁰ A semiempirical absorption correction was applied using the program SORTAV.⁵¹

For **1b** data collection was performed on a Oxford Diffraction Xcalibur Nova single crystal diffractometer, using Cu- $K\alpha$ radiation ($\alpha = 1.5418$ Å). Images were collected at a 65 mm fixed crystal-detector distance, using the oscillation method, with 1° oscillation and (1.5-10) s variable exposure time per image. Data collection strategy was calculated with the program CrysAlis Pro CCD.⁵² Data reduction and cell refinement was performed with the program CrysAlis Pro RED.⁵² An empirical absorption

Scheme 2. Synthesis of Complexes 1a–c and 2a–c



correction was applied using the SCALE3 ABSPACK algorithm as implemented in the program CrysAlis Pro RED.⁵²

In all cases the software package WINGX⁵³ was used for space group determination, structure solution, and refinement. The structures of complexes **1a** and **1c** were solved by Patterson interpretation and phase expansion using DIRDIF.⁵⁴ For **1b** the structure was solved by direct methods using SIR92.⁵⁵

Isotropic least-squares refinement on F^2 was performed using SHELXL97⁵⁶. During the final stages of the refinements, all the positional parameters and the anisotropic temperature factors of all the non-H atoms were refined. The H atoms for **1a** and **1c** (except H1A,B for **1a** and H1A,B, H10A,B, H24A,B for **1c**) were geometrically located, and their coordinates were refined riding on their parent atoms. For **1b**, H1A,B for **1a** and H1A,B, H10A,B, H24A,B for **1c**, the coordinates of H atoms were found from different Fourier maps and included in a refinement with isotropic parameters. The function minimized was $([\sum w(F_o^2 - F_c^2)] / \sum w(F_o^2))^{1/2}$ where $w = 1/[\sigma^2(F_o^2) + (aP)^2 + bP]$ (a and b values are collected in Supporting Information, Table S1) with $\sigma^2(F_o^2)$ from counting statistics and $P = (\max(F_o^2, 0) + 2F_c^2)/3$.

Atomic scattering factors were taken from the International Tables for X-ray Crystallography International.⁵⁷ Geometrical calculations were made with PARST.⁵⁸ The crystallographic plots were made with PLATON.⁵⁹

Computational Details. All the theoretical calculations have been performed using the density functional theory (DFT). The full catalytic cycles with complexes **1a–c** were computed with the Becke's three-parameter exchange functional (B3)^{60,61} in conjunction with the Lee–Yang–Parr correlation functional (LYP)^{62,63} as implemented in Gaussian 03.⁶⁴ To obtain more accurate values of the energy barriers of the hydrogen transfer steps these barriers were recalculated, with reoptimization of intermediates and transition states, using the M06 functional⁶⁵ with an ultrafine grid, as implemented in the Gaussian 09 program.⁶⁶ In all geometry optimizations the effective core potential LANL2DZ along with its associated basis set, complemented by a series of f polarization functions was employed for Ru,^{67,68} 6-31G(d) basis set was used for all the non-hydrogen atoms, 6-31G(d,p) for the hydrogen atoms of the aqua and pyrazole ligands, as well as the substrates, and 6-31G for the rest of hydrogen atoms.⁶⁸ Vibrational frequencies were computed to characterize the transition states and the minima, as well as for the calculation of gas-phase Gibbs energies. The connection between transition states and their corresponding reactants and products was checked by fully optimizing structures derived from the transition states with a small displacement following the transition vector in both directions.

The energies in solution (ΔE_{sol}) of all the species were estimated adding to the potential energy the contribution of the Gibbs energy of solvation by the application of single-point calculations, using the polarizable continuum model (PCM) with standard solvation spheres^{69–72} in H₂O, ($\epsilon = 78.4$) at the gas-phase optimized stationary points. An extended basis set, with a 6-311++G(d,p) description of all the atoms⁷³ but the ruthenium, described as LANL2DZ+f, was employed in these calculations. The ΔE_{sol} values include the Gibbs energy effects of the solvent, but not those of the solute. The Gibbs energies in solution (ΔG_{sol}) were calculated adding the gas-phase Gibbs energy corrections of the solute to the energies in solution. All the energies collected in the text are ΔG_{sol} . ΔE_{sol} profiles are shown in the Supporting Information.

RESULTS AND DISCUSSION

Synthesis of Imidazole-Based Ruthenium Complexes and Speciation in Aqueous Medium. We have investigated the catalytic activity of ruthenium(IV) $[\text{Ru}(\eta^3\text{-}\eta^3\text{-C}_{10}\text{H}_{16})\text{Cl}_2(\text{L})]$ (L = imidazole (**1a**), benzimidazole (**1b**), *N*-methylimidazole (**1c**)) and ruthenium(II) $[\text{Ru}(\eta^6\text{-arene})\text{Cl}_2\text{L}]$ complexes (**2a–c**) for comparative purposes. All of them have been synthesized in good yield from the commercially available dimeric precursors $[\{\text{Ru}(\eta^3\text{-}\eta^3\text{-C}_{10}\text{H}_{16})\text{Cl}_2\}_2]$ and $[\{\text{RuCl}(\mu\text{-Cl})(\eta^6\text{-arene})\}_2]$ by reaction with the appropriate ligand following procedures reported in the literature for analogous 1,2-azoles^{39,40} and for **2b,c**^{47,48} (Scheme 2).

All of them have been isolated as air-stable orange solids soluble in dichloromethane and acetone and insoluble in hexane and diethyl ether. Although conductivity measurements of acetone solutions show that they are no electrolytes, the molar conductivities found in water (177 (**1a**), 75(**1c**) and 190 (**2a**) $\Omega^{-1} \text{cm}^2 \text{mol}^{-1}$) indicate that dissociation processes to give cationic derivatives take place in solution (low solubility in water of **1b** precludes conductivity measurements). Moreover, aqueous solutions of **1a** and **1c** are acid (pH = 5.75). These data seem to indicate that water-chloride exchange processes along with proton dissociations may occur.

Detailed insights on the chemical speciation of **1a–1c** in aqueous media were obtained from in situ ESI mass spectrometry (following a protocol previously reported),⁴⁰ which are in accord with the conductivity data. Aqueous solutions of compounds **1a–1c** were stirred and aliquots were extracted at different time intervals, diluted with water to a final concentration of $5 \times 10^{-4} \text{ M}$ (based on the initial Ru concentration), and directly introduced to the mass spectrometer. As a representative example of the ESI mass of complex **1a** are provided in Supporting Information,

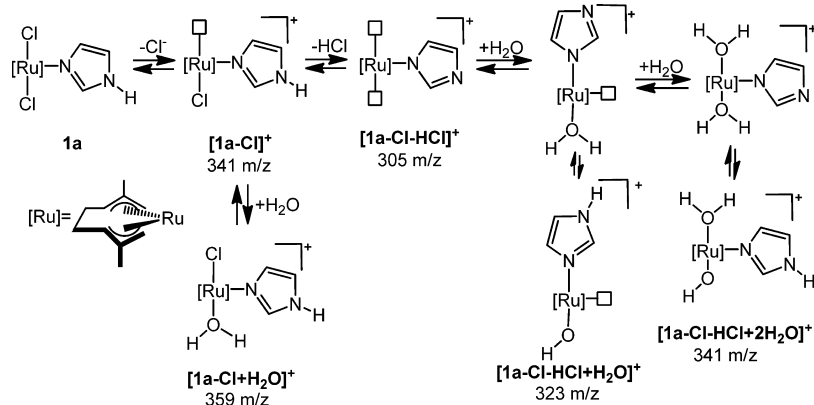
Scheme 3. Formation Equilibrium of Cationic Species Detected by ESI-MS of **1a** Aqueous Solution at $t = 0$ and $t = 1.5$ h

Figure S1 illustrating the temporal evolution of a freshly prepared aqueous solution at different time intervals.

At $t = 0$ h, the ESI mass spectrum shows a dominant species identified as $[1a - Cl]^+$ (m/z 341) accompanied by a minor peak assigned to $[1a - Cl + H_2O]^+$ (m/z 359) that formally correspond to the Ru–Cl cleavage and subsequent water coordination in the vacant site. This experimental evidence in combination with conductivity measurements strongly suggest that water speciation of **1a** at the early stages is dominated by singly charged $[1a - Cl]^+$ and $[1a - Cl + H_2O]^+$ species. An additional minor species at $m/z = 305$ is also observed and assigned to $[1a - Cl - HCl]^+$ on the basis of its m/z value as well as its isotopic distribution (Scheme 3). After 1 h, new species are detected in the ESI mass spectrum, arising from the evolution of the former aqua-species. Cationic chloride free species, namely, $[1a - Cl - HCl]^+$ (m/z 305), their corresponding mono- and disolvated species, namely, $[1a - Cl - HCl + H_2O]^+$ (m/z 323) and $[1a - Cl - HCl + 2H_2O]^+$ (m/z 341), were also detected and their relative intensity increase relative to the initial $[1a - Cl]^+$ (m/z 341). Note that species $[1a - Cl]^+$ and $[1a - Cl - HCl + 2H_2O]^+$ are overlapped; however, they could be unambiguously identified on the basis of their distinctive collision induced dissociation (CID) spectra.⁴⁰ Let us note that the versatility of the ESI-MS technique and its tandem version in transferring intact ions from the reaction solution to the gas phase is well-documented in the context of homogeneous catalytic reactions^{74–77} as further illustrated in the present work. Aqueous chemical speciation for compound **1b** and **1c** was comparable to that found for **1a** as judged by identical ESI-MS analysis (see Supporting Information).

Spectroscopic data (IR and NMR spectra) and elemental analysis for compounds **1a–c** and **2a** are in agreement with the proposed formulations (see Experimental Section for details). In particular, 1H and $^{13}C\{^1H\}$ NMR spectra of **1a–c** and **2a** show the signals for the η^3, η^3 -2,7-dimethylocta-2,6-diene-1,8-diyl and η^6 - C_6H_6 ligands respectively, which compare well with those previously reported for analogous complexes.^{40,78–81} As expected, proton and carbon resonances of the 2,7-dimethylocta-2,6-diene-1,8-diyl group in the NMR spectra are in accordance with the formation of a simple equatorial adduct with a C_2 symmetry in which the two halves of the bis-allyl ligand are in equivalent environments.⁸² In addition, the structures of ruthenium(IV) complexes **1a–c** were unequivocally confirmed by a single crystal X-ray diffraction study. Drawings of the molecular structures including selected bond distances and angles are depicted in the Supporting Information, Figure S2.⁸³

Catalytic Activity of Imidazole Based Ruthenium Complexes for the Isomerization of Allylic Alcohols In Water. Figure 1 shows the catalytic activity of ruthenium(IV)

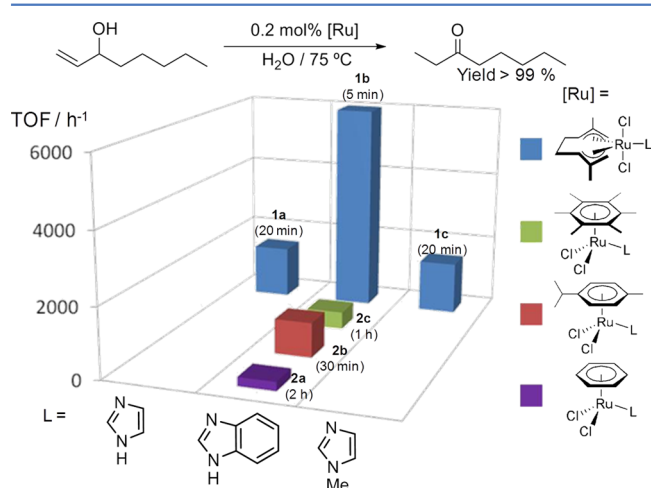


Figure 1. Isomerization of 1-octen-3-ol into octa-3-one catalyzed by complexes **1a–c** and **2a–c** in water. Reactions performed under N_2 atmosphere using 4 mmol of 1-octen-3-ol (0.2 M). Substrate/Ru = 500/1. Yield of octa-3-one determined by GC. Turnover frequencies ((mol product/mol Ru)/time) were calculated at the time indicated in each case.

(**1a–c**) and ruthenium(II) (**2a–c**) complexes for the isomerization of 1-octen-3-ol into octa-3-one in water and in the absence of base as a reaction model. Under the optimized reaction conditions previously reported for analogous catalysts (i.e., 0.2 M of 1-octen-3-ol, 0.2 mol % in Ru, heating at 75 °C in water)^{24–29,39,40} all the catalysts turned out to be active, although ruthenium(IV) precatalysts show much higher activity than ruthenium(II) derivatives⁸⁴ reaching quantitative transformations in only 5–20 min vs 30–180 min for the latter. We were pleased to find that complex **1b** displays much higher catalytic activity than **1a** and **1c**, leading to quantitative transformations in less than 5 min. This outstanding catalytic performance is maintained at room temperature (100 min; >99% yield)⁸⁵ and most interestingly under a lower catalyst loading (0.02 mol %) reaching an excellent yield of 3-octanone (>99%) in only 5 min. (TOF = 60,000 h^{-1}).⁸⁶ This methodology is also amenable for practical applications in a multigram scale in which 20 mmol (2.68 g) of α -vinylbenzyl alcohol is isomerized by **1b** (1 mol %) into 1-phenylpropan-1-one after 15 min at 75 °C (isolated yield 89%).

Complex **1b** is also very efficient in the isomerization of a range of allylic alcohols proving the wide scope and limitations of this catalytic transformation. The results are shown in Table 1. There

Table 1. Isomerization of Substituted Allylic Alcohols Catalyzed by Complex **1b in Water at 75 °C^a**

entry	substrate	Product	mol% [Ru]	time	Yield (%) ^b
1 ^c			0.2	5 min	>99
2			0.2	15 min	99
3			0.2	15 min	99
4			0.2	30 min	97
5			0.2	30 min	99
6			0.2	30 min	90
7			1	15 min	>99
8			10	2 h	83
9			5	1.5 h	99
10			5	0.5 h	99
11			5	2.5 h	62 ^d
12			10	15 h	99
13			10	2 h	87

^aReactions performed under N₂ atmosphere using 1 mmol of allylic alcohol (0.2 M). ^bYields determined by GC. ^c[Cycle] and Accumulative TON (mol product/mol Ru): [1st] 99; [2nd] 198; [3rd] 297; [4th] 396; [5th] 495; [6th] 592; [7th] 691. ^d12% of α,β -unsaturated aldehyde (cinnamaldehyde).

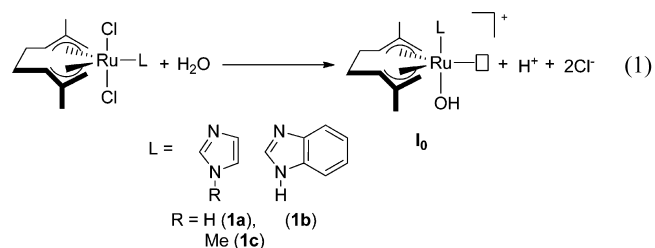
is a strong dependence upon the substitution of the carbon-carbon double bond, a behavior previously reported with other catalytic systems.^{6–29} Thus, monosubstituted aliphatic olefins 1-hepten-3-ol, 1-hexene-3-ol, 1-pentene-3-ol, 3-buten-2-ol, and 2-propen-1-ol are readily isomerized in 15–30 min (90–99% yield, entries 1–5).⁸⁷ In contrast, when either 1,1- or 1,2-disubstituted allylic alcohols are used, longer reaction times and higher catalyst loadings (1–10 mol %) are required to achieve high conversions (entries 7–13). Remarkably, the catalyst **1b** has shown a high capacity to be recycled remaining active up to seven cycles (entry 1^c).

Bifunctional Catalysis without Participation of N-H Protic Groups: Mechanistic Considerations. Our previous study on allylic alcohol isomerization in water catalyzed by pyrazole-based ruthenium complexes (Scheme 1) raised doubts about the need for an NH moiety in the ligand to perform a metal-ligand cooperating bifunctional catalysis of such process. The experimental results reported above show that similar or even improved catalytic efficiencies can be obtained with imidazole and benzimidazole complexes **1a** and **1b** in which the orientation of the β -N-H unit of the ligands make them unsuitable to participate in proton transfer to/from the substrate. To confirm the key role that water ligands can play as alternative to N-H Noyori type ligands in bifunctional catalyzed processes in water, we have carried out a DFT study of the isomerization of 2-propen-1-ol by imidazole-based complexes **1a**, **1b**, and **1c**, using a similar approach to that employed

for pyrazole-based complexes. The previous study pointed out a crucial role of hydroxo species generated by deprotonation of the corresponding aqua-complexes (Chart 2). Thus, hydroxo species with imidazole (**OH-a-I₀**), benzimidazole (**OH-b-I₀**), and methylimidazole (**OH-c-I₀**) will be considered as the active species. For all the hydroxo complexes we have found two pathways with relative cis- (**c-**) and trans- (**t-**) arrangement of the hydroxo and imidazole ligands. The catalytic cycle has been investigated with both isomers for the three hydroxo-complexes.

The previous study involving pyrazole catalysts showed that the overall isomerization implies two-hydrogen transfer steps: from the substrate to the catalyst (dehydrogenative step) and subsequent transfer back to the substrate (acrolein hydrogenation) disclosing an outer-sphere bifunctional catalyzed mechanism for both processes (Scheme 1). In the first step (path A) hydrogen transfer to the Ru/OH moiety occurs while a cooperative action of the metal and the pyrazole ligand takes place in the second step (hydrogenation from the Ru-H/pyrazole N-H moiety; path B). Calculations also demonstrated that the second half of the reaction has a considerably lower barrier when the acrolein hydrogenation takes place via 1,4-addition, forming initially the enol (1-propen-1-ol) instead of a direct C=C reduction. The enol can be easily isomerized to propanal in water. With this in mind, we have explored the isomerization mechanism with the imidazole-based catalysts considering the water ligand formed by protonation of the hydroxo ligand in the first step is acting as the proton transfer agent in the hydrogenation in a similar way as described for pyrazole complexes. Schemes 4 and 5 show the catalytic cycles investigated with the trans- (*trans-hydroxo route*) and cis- (*cis-hydroxo route*) isomers of the hydroxo-imidazole active species **t-OH-a-I₀** and **c-OH-a-I₀**, respectively (for catalytic cycles with the corresponding active species of the benzimidazole and *N*-methylimidazole complexes see the Supporting Information, Schemes S1–S4).

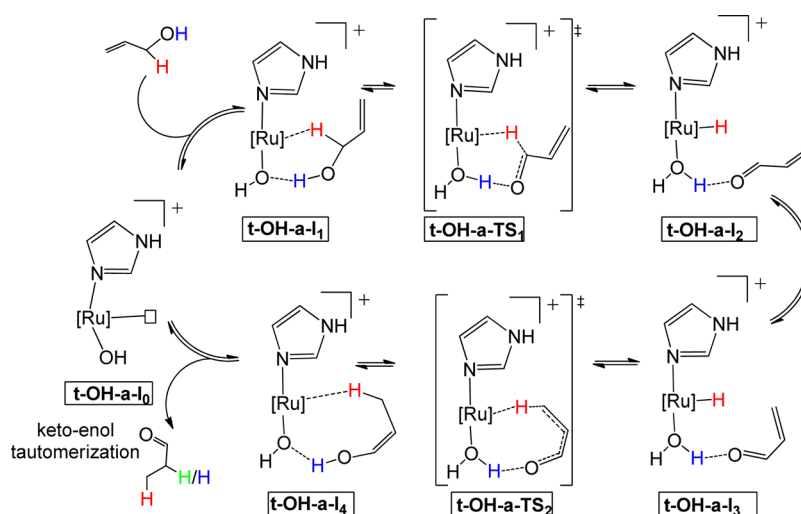
Accessibility of Hydroxo-Imidazole Active Species. An essential point in the proposed mechanism is the existence in water of the hydroxo active species cis- and trans- hydroxo complexes (Scheme 6). To discuss more quantitatively the accessibility of such species from the neutral dichloro complexes we have estimated their relative Gibbs energies in water using eq 1.



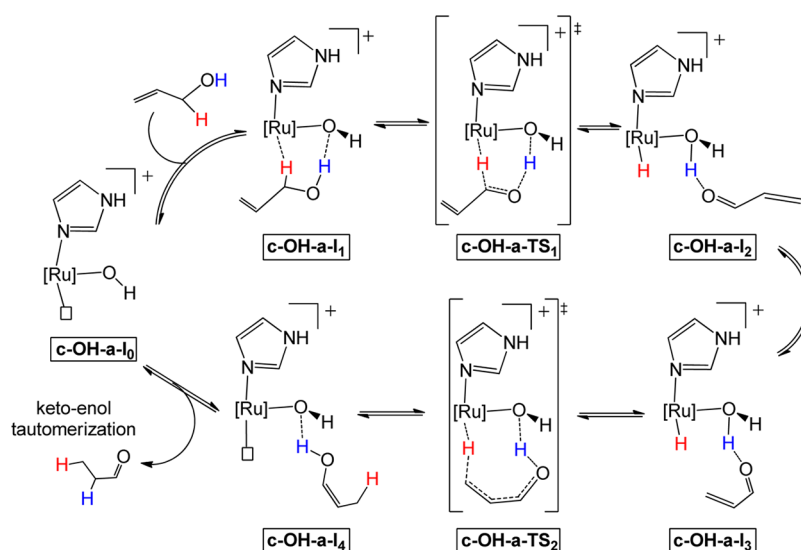
To calculate these values, experimentally derived values for the aqueous solvation Gibbs energy of a proton ($-264.0 \text{ kcal mol}^{-1}$)⁸⁸ and a chloride ion ($-74.6 \text{ kcal mol}^{-1}$)⁸⁹ have been used. The calculated relative energies should be considered an estimation given the inherent difficulties in calculating solvation energies of charged species. For all the hydroxo complexes both cis- and trans- isomers have very similar energies (Scheme 6).

The hydroxo complexes are found in the range from about 13 to 16 kcal mol⁻¹ above the neutral saturated dichloro complexes. These values are lower than those calculated for the analogous cis- and trans- hydroxo pyrazole complexes (18.3 and 20.1 kcal mol⁻¹, respectively). Moreover, whereas in the pyrazole-based system the cis-aqua/pyrazolide complex is 3.8 kcal mol⁻¹

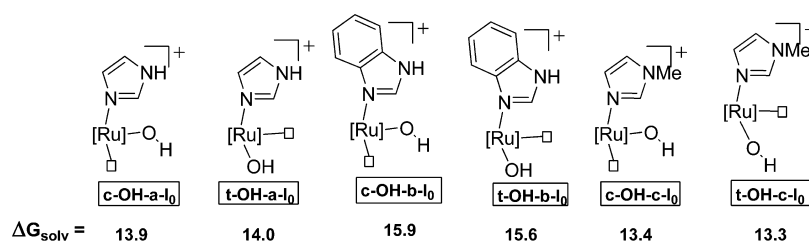
Scheme 4. Proposed Catalytic Cycle for the Isomerization of 2-Propen-1-ol into Propanal in Water Promoted by *t*-OH-a-I₀ (*trans*-hydroxo route for 1a)



Scheme 5. Proposed Catalytic Cycle for the Isomerization of 2-Propen-1-ol into Propanal in Water Promoted by *c*-OH-a-I₀ (*cis*-hydroxo route for 1a)

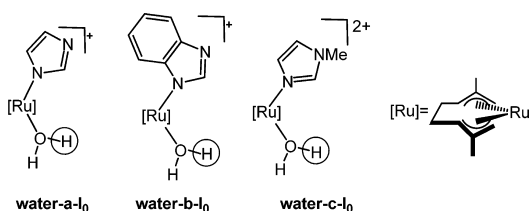


Scheme 6. Relative Gibbs Energies in Water (kcal mol⁻¹), with Respect to the Parent Dichloro Complexes, of the *cis*- and *trans*-Hydroxo Complexes



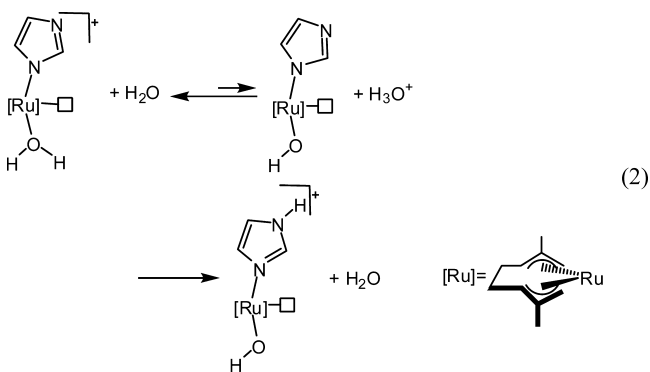
more stable than the *trans*-hydroxo/pyrazole active species, in the imidazole-based complexes the *cis*-aqua/imidazolide is 8.5 kcal mol⁻¹ less stable than the *trans*-hydroxo/imidazole and the aqua/benzimidazolide and hydroxo/benzimidazole complexes are isoenergetic. Overall the data point out an easier formation and higher concentration of the hydroxo active species in the imidazole-based complexes than in the pyrazole-based partners.

To further assess the presence of hydroxo complexes in aqueous solutions of **1a**, **1b**, and **1c** we have calculated, using the M06 functional,⁶⁵ the pK_a of the coordinated water in the cationic species formed by water-chloride exchange and that have been detected by ESI-MS (for instance, for **1a**: [**1a** - Cl - HCl + H₂O]⁺ *m/z* 323, see Scheme 3). To this end we have estimated the Gibbs energy of deprotonation in water ($\Delta G_{\text{sol},\text{deprot}}^{\circ}$) of the aqua-complexes **water-a-I₀**, **water-b-I₀**, and **water-c-I₀** (Scheme 7)

Scheme 7. Aqua-Complexes Considered in the pK_a Calculations

using the thermodynamic cycle we have already employed for the estimation of pK_a 's of organometallic complexes (see Supporting Information).⁹⁰ From this value, calculation of pK_a is straightforward ($pK_a = \Delta G^{\circ}_{\text{solv,deprot}}/2.303RT$). Details of the pK_a calculations are given in the Supporting Information. We checked the suitability of such an approach for calculating the pK_a of the free imidazole and benzimidazole molecules. The obtained results (14.3 and 12.5, respectively) are in very good agreement with the experimental values (14.2 and 12.75). The $\Delta G^{\circ}_{\text{solv,deprot}}$ of the aqua-complexes are $13.7 \text{ kcal mol}^{-1}$ ($L = \text{imidazole}$), $16.0 \text{ kcal mol}^{-1}$ ($L = \text{benzimidazole}$), and $13.5 \text{ kcal mol}^{-1}$ ($N\text{-methyl imidazole}$). Accordingly, the calculated pK_a for the coordinated water in aqua-complexes **water-a-I₀**, **water-b-I₀**, and **water-c-I₀** are 10.1 (imidazole), 11.9 (benzimidazole), and 10 (methylimidazole).

Comparing these values with that of a water molecule in pure water (15.7), it is apparent that a significant increase in the acidity of water (about 5 pK_a units) can be recognized. The pK_a decrease places coordinated water in an acidity strength similar to that of phenol ($pK_a = 9.9$), for which phenolate anion exists in appreciable concentration in water. Moreover, the presence of a basic iminic N atom of the ligand allows the proton dissociation and subsequent protonation of the resulting neutral hydroxo complex (proton transfer). This leads to a more stable product, which displaces the overall deprotonation-protonation equilibrium toward the formation of the hydroxo complexes proposed to be the active species (eq 2).



ESI-MS detected a $[\mathbf{1a} - \text{Cl} - \text{HCl} + \text{H}_2\text{O}]^+$ species (m/z 323). Both the aqua/imidazolide and the hydroxo/imidazole formulations are compatible with this m/z value. Calculations support the hydroxo-imidazole nature of such species. Therefore it seems very likely that the presence in aqueous solution of the hydroxo-complexes derived from **1a–c** species, proposed to be the active species in the isomerization process.

Catalytic Efficiency in Water of the β -N-H Protic Imidazole Based and *N*-methylimidazole Ruthenium(IV) Complexes. We have computed the full catalytic cycles for the isomerization of allylic alcohol in water assuming the cationic trans- and cis-hydroxo complexes derived from **1a**, **1b**, and **1c**

(Scheme 6) behave as active species. The Gibbs energy profiles in water for the isomerization catalyzed by trans- and cis-hydroxo complexes **t-OH-a-I₀** and **c-OH-a-I₀** (trans- and cis-hydroxo routes, catalytic cycles outlined in Schemes 4 and 5, respectively) are presented in Figure 2. The catalytic cycles and Gibbs energy profiles for the isomerization reaction catalyzed by the cis- and trans- hydroxo derivatives formed in aqueous solution from benzimidazole (**1b**) and *N*-methylimidazole (**1c**) complexes are very similar to those of the related imidazole species and are collected in the Supporting Information, Figures S11 and S13, respectively.⁹¹

The isomerization takes place through two sequential concerted hydrogen transfers with a cooperative action of the metal and the hydroxo ligand. The imidazole ligand is first accepting a proton from the 2-propen-1-ol substrate (dehydrogenation step) and then the aqua ligand formed in this way is transferring back the proton to the acrolein. (hydrogenation step). At the same time a hydride is transferred to and from the metal, giving rise to the enol form of the product. Transition states for the hydrogen transfer steps with selected structural parameters are shown in Figure 3.

The Gibbs energy barriers for the dehydrogenative step are $16.6 \text{ kcal mol}^{-1}$ in the trans-hydroxo route and $21.3 \text{ kcal mol}^{-1}$ in the cis-hydroxo route. At this point acrolein has been formed, and the catalyst has achieved its reduced form, which will transfer two hydrogens to acrolein in the second half of the reaction. Acrolein hydrogenation is markedly more asynchronous than 1-propen-1-ol hydrogenation, hydride transfer being much more advanced than the proton transfer in the transition state of this step.⁹² Regarding the reduced form of the catalyst, the cis-aqua ruthenium hydride is considerably more stable than the parent trans-aqua ($10.5 \text{ kcal mol}^{-1}$). This fact places the energy profile for the acrolein hydrogenation in the trans-hydroxo route above that of the cis-hydroxo pathway (Figure 2). However the energy barriers for this step, computed from the respective intermediates (**t-OH-a-I₂** and **c-OH-a-I₂**) are very similar: 11.6 and $12.0 \text{ kcal mol}^{-1}$ for the trans- and cis-routes, respectively. Overall the isomerization catalyzed by the trans-hydroxo active species is favored by $3.6 \text{ kcal mol}^{-1}$ over that involving the cis-hydroxo species (global barriers⁹³ of 17.6 and $21.3 \text{ kcal mol}^{-1}$).

The results discussed above stress the feasibility of the bi-functional catalysis with cooperative action of a water ligand for the ruthenium-catalyzed isomerization of allylic alcohols in water. However, hydrogen-bonding interactions between the reactive system and the water medium, not accounted for with a continuum description of the solvent, could affect the energy barriers.⁹⁴ To check whether by improving the solvent model could affect our results, we have recalculated the energy barriers of the two hydrogen transfer steps (transition states **TS1** and **TS2**) in the trans-hydroxo route with an improved description of solvent effects. In this model, explicit water molecules (from one to four) able to establish hydrogen-bonding interactions with the catalyst and the substrate have been included, in addition to the continuum description of the solvent. The calculated Gibbs energy barriers, depending on the number of explicit water molecules, are collected in Table 2. Geometries of the transition states with explicit water molecules are presented at the Supporting Information and Scheme 8 (three water molecules as illustration).

As it is sketched in Scheme 8 for the model with three explicit water molecules, a network of hydrogen bonds is connecting the substrate and the hydroxo ligand in the transition states of the first and second hydrogen transfer, and a water molecule is also

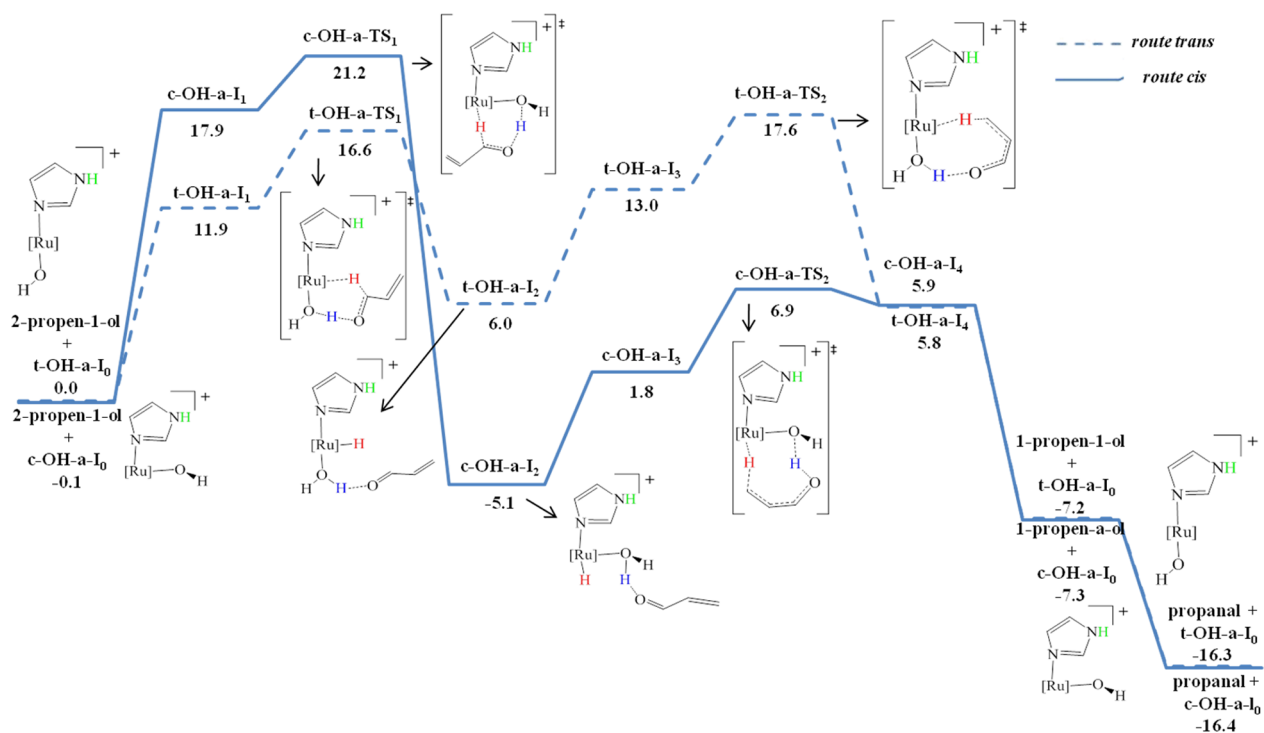


Figure 2. Gibbs energy profiles in water for the isomerization of 2-propen-1-ol into propanal assuming *trans*-[Ru(η^3 : η^3 -C₁₀H₁₆)(OH)(imidazole)]⁺ (**t-OH-a-I₀**) and *cis*-[Ru(η^3 : η^3 -C₁₀H₁₆)(OH)(imidazole)]⁺ (**c-OH-a-I₀**) are the active species (*trans*- and *cis*-hydroxo route for **1a**). The values are in kcal mol⁻¹ and referred to the separated reactants **t-OH-a-I₀** and 2-propen-1-ol.

hydrogen bonded to the β -N-H protic group of the 1,3-azole ligand. Although the presence of explicit water molecules modifies the energy barriers, the global barriers obtained with the most accurate models (including three or four explicit solvent molecules) differ less than 1 kcal mol⁻¹ from that obtained with the purely continuum model. Thus, we can conclude that the feasibility of a bifunctional-catalyzed mechanism with participation of an aqua ligand for hydrogen-transfer processes in aqueous medium is kept when a cluster of explicit solvent molecules is included in the calculations. Note that the results with only one explicit water molecule deviate notably from those with larger water clusters, pointing out that smaller water cluster could give skewed results.

The calculated barriers for the two hydrogen transfer steps assuming the hydroxo complexes of the three imidazole based ruthenium(IV) complexes take part as the active species in the isomerization of 2-propen-1-ol into propanal are gathered in Table 3. The B3LYP results outline lower barriers for the *trans*-hydroxo routes than for the *cis*-hydroxo ones, as well as lower barriers for the second hydrogen transfer (hydrogenation step) than for the first one (dehydrogenation step). The overall barriers for the favored *trans*-hydroxo routes with the three imidazole based complexes although similar follow the order **1b** < **1a** < **1c** (imidazole: 17.6 kcal mol⁻¹; benzimidazole: 17.0 kcal mol⁻¹; *N*-methylimidazole: 18 kcal mol⁻¹). We have also included in Table 3 the barriers already reported for the pyrazole complex.⁴⁰ The global barrier for the 2-propen-1-ol isomerization with this catalyst is the lowest one, in seeming contradiction with its lowest catalytic efficiency. However there is an important feature of the hydroxo catalysts not reflected in Table 3: its relative energy with respect the parent aqua complex initially formed by chloride dissociation. This issue determines the effective concentration of the active species in the reaction medium. Whereas for the hydroxo/imidazole-based complexes

the *cis*-aqua-imidazolide is less stable than the *cis*-hydroxo/imidazole (isoenergetic for the corresponding benzimidazole complexes), the hydroxo-pyrazole active species is found 3.8 kcal mol⁻¹ above its aqua-pyrazolide isomer.⁴⁰ Thus, adding the energy required to forming the active species to the global barrier the value obtained for the pyrazole complex is 19.1 kcal mol⁻¹, which is the highest one in the series. Therefore, calculations point out an important role of the availability of the hydroxo species in the catalytic efficiency of these species.

The B3LYP computed barriers seem to be too high, according to the experimentally determined TOF. Because recent studies have established that the M06 functional predicts the activation energies more accurately than B3LYP,⁶⁵ we have recalculated the Gibbs energy barriers in water for catalysts **1a–1c**, as well as for the pyrazole complex, using the M06 functional. The geometries of the transition states for both hydrogen transfers and their most stable preceding intermediates have been reoptimized with this functional and are included in the Supporting Information. Although changes in the geometries are minor, notable changes in the barriers take place when changing the B3LYP functional by the M06, which describe more accurately non covalent interactions such as those occurring in the transition states of the hydrogen transfer steps. As shown in Table 3, the M06 global barriers are about 3.5 kcal mol⁻¹ lower than the B3LYP ones, in better agreement with the catalytic activity of the imidazole based ruthenium complexes. The M06 global barriers for the three imidazole based complexes are very similar ((imidazole: 13.8 kcal mol⁻¹; benzimidazole: 13.9 kcal mol⁻¹; *N*-methylimidazole: 13.6 kcal mol⁻¹) suggesting that the slight differences in the barriers, which are at the origin of the differences in TOF between **1a–1c** complexes, are out of the accuracy of the calculations. M06 calculations also point out much closer barriers for the *cis*- and *trans*-hydroxo routes and for the first and second hydrogen transfers.

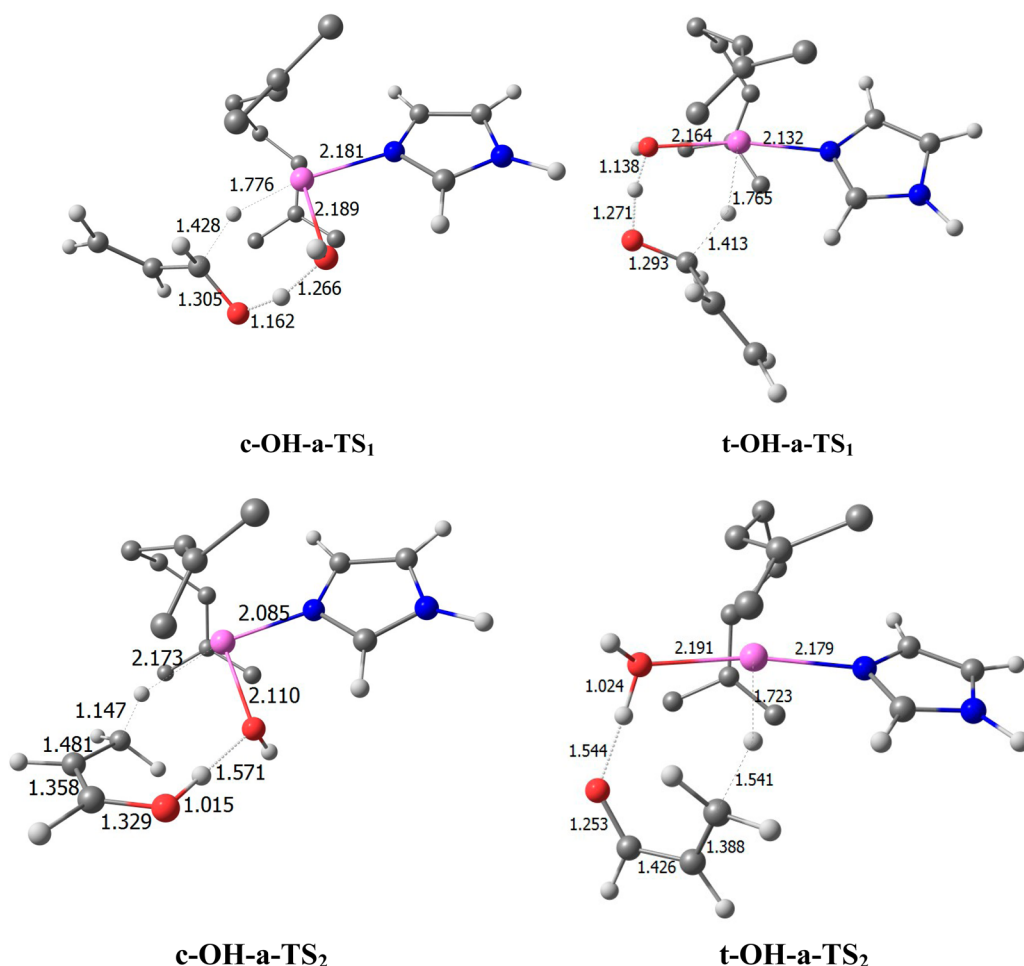


Figure 3. Transition states for the hydrogen-transfer steps in the isomerization of 2-propen-1-ol into propanal catalyzed by **1a** in the cis- and trans-hydroxo routes. Hydrogen atoms in the bis(allyl) ligand have been omitted for clarity.

Table 2. Gibbs Energy Barriers (kcal mol⁻¹) for the Two Hydrogen Transfer Steps in the Isomerization of 2-Propen-1-ol into Propanal in Water Catalyzed by **1a** with Explicit Solvent Molecules Included in the Calculated System

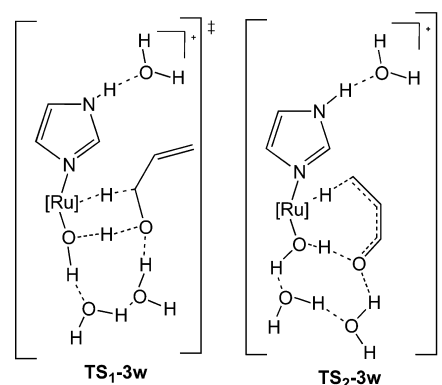
number of explicit water molecules	1 st hydrogen transfer ^a	2 nd hydrogen transfer ^a	global barrier ^b
0	16.6	11.6	17.6
1	12.4	13.3	14.4
2	16.6	14.2	18.8
3	16.7	12.7	16.7
4	18.4	9.8	18.4

^a $\Delta G_{\text{water}}^{\ddagger}$ barriers from the most stable preceding intermediate.

^bDefined as the Gibbs energy difference between the highest and the lowest structures along the whole catalytic cycle, ref 93.

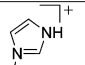
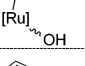
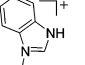
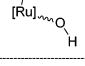
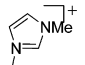
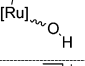
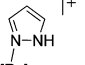
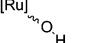
Overall, the barriers found with the three imidazole based complexes underline the viability of a mechanism relying on the key role of a water ligand acting as cooperating ligand along the catalytic cycle. In our previous report, using pyrazole-based ruthenium complexes, we gave evidence that the hydroxo complex could take part in the dehydrogenative half of the reaction, but protonation from the pyrazole ligand was favored over protonation from the aqua ligand (see Scheme 1).⁴⁰ The present results demonstrate that in water the participation of the N-H group of the azole ligand in the bifunctional catalysis

Scheme 8. Transition States for the Hydrogen-Transfer Steps in the trans-Hydroxo Route Catalyzed by t-OH-a-I₀ with Three Additional Water Molecules



process is not required, provided that a water ligand could play the same role. In this sense, the catalytic action of the *N*-methylimidazole complex, where both nitrogen atoms of the ring are substituted, is particularly appealing. Indeed, the TOF obtained with the benzimidazole complex **1b** (much higher than that shown by the partner pyrazole complex) prove that a higher catalytic efficiency can be achieved without direct intervention of the azole ligands.

Table 3. Calculated Gibbs Energy Barriers for Each Hydrogen Transfer Step and Global Barrier^a for the Isomerization of 2-Propen-1-ol into Propanal in Water Using Different Pre-Catalysts with 1,3-Azole Ligands (kcal mol⁻¹; in italics, M06 values)

Pre-catalyst	Ligand	Active species	1 st Hydrogen transfer ^b	2 nd Hydrogen transfer ^b	Global Barrier ^a
1a	imidazole	 <i>trans</i> -OH	16.6 <i>[13.4]</i>	11.6 <i>[11.4]</i>	17.6 <i>[13.8]</i>
		 <i>cis</i> -OH	21.3 <i>[13.8]</i>	12.0 <i>[15.3]</i>	21.3 <i>[15.3]</i>
1b	benzimidazole	 <i>trans</i> -OH	17.0 <i>[13.5]</i>	12.1 <i>[13.2]</i>	17.0 <i>[17.3]</i>
		 <i>cis</i> -OH	18.5 <i>[13.9]</i>	15.0 ^c <i>[11.1]</i>	18.5 <i>[13.9]</i>
1c	N-methylimidazole	 <i>trans</i> -OH	17.2 <i>[12.9]</i>	14.3 <i>[12.2]</i>	18.0 <i>[14.2]</i>
		 <i>cis</i> -OH	20.9 <i>[13.6]</i>	14.1 <i>[11.7]</i>	20.9 <i>[13.6]</i>
3a	pyrazole	 <i>trans</i> -OH	15.3 ^d <i>[12.9]</i>	8.0 ^d <i>[5.9]</i>	15.3 ^d <i>[12.9]</i>
		 <i>cis</i> -OH	20.4 ^d <i>[10.9]</i>	12.3 ^d <i>[13.4]</i>	20.4 ^d <i>[13.4]</i>

^aDefined as the Gibbs energy difference between the highest and the lowest structures along the whole catalytic cycle, ref 93. ^b $\Delta G_{\text{water}}^{\ddagger}$ barriers from the most stable preceding intermediate. ^cStepwise process with two transition states (first hydride addition, then protonation). ^dRef 40.

CONCLUSIONS

In this work, we have shown that the bis-allyl ruthenium(IV) complexes containing 1,3 azole β -N-H protic ligands [Ru(η^3 : η^3 -C₁₀H₁₆)Cl₂L] (C₁₀H₁₆ = 2,7-dimethylocta-2,6-diene-1,8-diyl) (L = imidazole (**1a**), benzimidazole (**1b**)), N-methylimidazole (**1c**), are highly efficient precatalysts for the redox isomerization of allylic alcohols into carbonyl compounds in aqueous medium and in the absence of base. In particular, complex **1b** displays much higher catalytic activity than **1a** and **1c** leading to quantitative transformations of 1-octen-3-ol in less than 5 min. This outstanding catalytic performance is maintained at room temperature and most interestingly under a low catalyst loading (0.02 mol %) reaching a quantitative yield in only 5 min (TOF = 60,000 h⁻¹). To the best of our knowledge, this is the most efficient catalyst reported to date in water. Moreover, catalyst **1b** can be recycled, remaining active up to seven cycles. These results show that the presence of a N-H group is not required to catalyze the isomerization. In this sense, the catalytic action of the N-methylimidazole complex, where both nitrogen atoms of the ring are substituted, is particularly appealing.

DFT calculations give evidence that the hydroxo-complexes derived from **1a–c** species can be formed in aqueous solution. The theoretical study has also addressed the mechanism of action of a bifunctional catalyst in water in which the uncoordinated N-H group of imidazole remains unchanged, acting as a spectator ligand during the whole catalytic cycle. In this mechanism the hydroxo complex is the catalytic active species, acting as cooperative ligand in the same way that α -N-H groups do in mechanisms of conventional bifunctional catalysis. Our results demonstrate that in water the participation of the β -N-H protic group of the 1,3-azole ligands in the bifunctional catalysis is not required, provided that a water molecule could play the same role.

Our study shows that, despite that these ligands featuring β -N-H protic groups are not required for the hydrogen transfer reactions, they play an important role in the fine-tuning of the ruthenium environment for the catalyst to attain its optimal efficiency. Efficient catalysis of the allylic alcohol isomerization entails both hydrogen transfers to and from the catalyst. Thus, a good catalyst should be able to perform efficiently both processes, which could require contrasting properties (for instance, formation of a too strong M-H bond in the first step would hamper the hydride transfer back to the substrate in the second step or a too acidic water ligand would make difficult the protonation of the hydroxo ligand in the second half of the process). Two key issues are related with the donor properties of the N-ligand: the acidity of the water ligand, which affects the concentration of the hydroxo active species, and the Lewis acid properties of the ruthenium center, which make it suitable for accepting the hydride. The donor properties of the benzimidazole ligand fit very well with the system requirements to reach an optimal performance in the allylic alcohol isomerization process. The results reported in the present work pave the way for the design of new bifunctional catalyzed processes in water in which aqua ligands act as the cooperating ligand.

ASSOCIATED CONTENT

Supporting Information

ESI mass spectra of aqueous solutions of compound **1a**. Crystallographic structures and data for compounds of **1a–c**. Proposed catalytic cycle and Gibbs energy profiles for the isomerization of 2-propen-1-ol promoted by **1b** and **1c** complexes. Energy profiles in water (ΔE_{water}). Optimized structures of all the minima and transition states. Details of the pK_a calculations. Complete authors' list for references 64 and 66. Cartesian coordinates and absolute energies and Gibbs energies (in hartrees) of all the calculated species. This material is available free of charge via the Internet at <http://pubs.acs.org>.

AUTHOR INFORMATION

Corresponding Author

*E-mail: jgh@uniovi.es (J.G.), agusti@klngon.uab.es (A.LL).

Funding

Financial support from the Spanish MICINN (projects CTQ2011-23336, CTQ2006-08485/BQU, and ORFEO Consolider-Ingenio 2010 CSD2007-00006) is gratefully acknowledged.

Notes

The authors declare no competing financial interest.

ACKNOWLEDGMENTS

The authors are grateful to the Serveis Centrals d'Instrumentació Científica (SCIC) of the Universitat Jaume I for providing us with mass spectrometry facilities. CESCA is acknowledged for providing computational resources.

REFERENCES

- (1) Van der Drift, R. C.; Bouwman, E.; Drent, E. *J. Organomet. Chem.* **2002**, *650*, 1–24.
- (2) Uma, R.; Crévisy, C.; Grée, R. *Chem. Rev.* **2003**, *103*, 27–51.
- (3) Cadierno, V.; Crochet, P.; Gimeno, J. *Synlett* **2008**, 1105–1124.
- (4) For more recent reviews see: Mantilla, L.; Mazet, C. *Chem. Lett.* **2011**, *40*, 341–344, and refs 5, 6.
- (5) Ahlsten, N.; Bartoszewicz, A.; Martín-Matute, B. *Dalton Trans.* **2012**, 1660–1670.
- (6) Lorenzo-Luis, P.; Romerosa, A.; Serrano-Ruiz, M. *ACS Catal.* **2012**, *2*, 1079–1086.

- (7) Joó, F. In *Aqueous Organometallic Catalysis*; Kluwer: Dordrecht, The Netherlands, 2001.
- (8) *Aqueous Phase Organometallic catalysis*; Cornils, B., Herrmann, W. A., Eds.; Wiley-VCH: Weinheim, Germany, 2004.
- (9) *Multiphase Organometallic Catalysis*; Cornils, B., Herrmann, W. A., Vogt, I., Eds.; Wiley-VCH: Weinheim, Germany, 2005.
- (10) Li, C.-J. *Chem. Rev.* **2005**, *105*, 3095–3165.
- (11) Chen, L.; Li, C.-J. *Adv. Synth. Catal.* **2006**, *348*, 1459–1184.
- (12) *Organic Reactions in Water*; Lindstrom, U. M., Ed.; Blackwell Publishing: Oxford, U.K., 2007.
- (13) McGrath, D. V.; Grubbs, R. H.; Ziller, J. W. *J. Am. Chem. Soc.* **1991**, *113*, 3611–3613.
- (14) Karlen, T.; Ludi, A. *Helv. Chim. Acta* **1992**, *75*, 1604–1605.
- (15) Bricout, H.; Monflier, E.; Carpentier, J. F.; Mortreux, A. *Eur. J. Inorg. Chem.* **1998**, 1739–1744.
- (16) Schumann, H.; Ravindar, V.; Meltser, L.; Baidossi, W.; Sasson, Y.; Blum, J. *J. Mol. Catal. A* **1997**, *118*, 55–61.
- (17) de Bellefon, C.; Caravieilhès, S.; Kuntz, E. G. *C. R. Acad. Sci., Ser. IIc: Chim.* **2000**, *3*, 607–614.
- (18) Bianchini, C.; Meli, A.; Oberhauser, W. *New J. Chem.* **2001**, *25*, 11–12.
- (19) Knight, D. A.; Schull, T. L. *Synth. Commun.* **2003**, *33*, 827–831.
- (20) Fekete, M.; Joó, F. *Catal. Commun.* **2006**, *7*, 783–786.
- (21) Campos-Malpartida, T.; Fekete, M.; Joó, F.; Kathó, A.; Romerosa, A.; Saoud, M.; Wojtków, W. *J. Organomet. Chem.* **2008**, *693*, 468–474.
- (22) Ahlsten, N.; Lundberg, H.; Martín-Matute, B. *Green Chem.* **2010**, *12*, 1628–1633.
- (23) Liu, P. N.; Ju, K. D.; Lau, C. P. *Adv. Synth. Catal.* **2011**, *353*, 275–280.
- (24) Cadierno, V.; Crochet, P.; García-Garrido, S. E. *Dalton Trans.* **2004**, 3635–3641.
- (25) Cadierno, V.; García-Garrido, S. E.; Gimeno, J.; Varela-Álvarez, A.; Sordo, J. A. *J. Am. Chem. Soc.* **2006**, *128*, 1360–1370.
- (26) Crochet, P.; Díez, J.; Fernández-Zumel, M. A.; Gimeno, J. *Adv. Synth. Catal.* **2006**, *348*, 93–100.
- (27) Díaz-Álvarez, A. E.; Crochet, P.; Zablocka, M.; Duhayon, C.; Cadierno, V.; Gimeno, J.; Majoral, J. P. *Adv. Synth. Catal.* **2006**, *348*, 1671–1679.
- (28) Crochet, P.; Fernández-Zumel, M. A.; Gimeno, J.; Scheele, M. *Organometallics* **2006**, *25*, 4846–4849.
- (29) Lastra-Barreira, B.; Díez, J.; Crochet, P. *Green Chem.* **2009**, *11*, 1681–1686.
- (30) For other ruthenium catalyzed processes in aqueous medium see refs 30–38 and 3: Cadierno, V.; García-Garrido, S. E.; Gimeno, J. *Chem. Commun.* **2004**, 232–233.
- (31) Cadierno, V.; García-Garrido, S. E.; Gimeno, J.; Nebra, N. *Chem. Commun.* **2005**, 4086–4088.
- (32) Cadierno, V.; García-Garrido, S. E.; Gimeno, J. *J. Am. Chem. Soc.* **2006**, *128*, 15094–15095.
- (33) Cadierno, V.; Francos, J.; Gimeno, J. N. *Chem. Commun.* **2007**, 2536–2538.
- (34) Cadierno, V.; Gimeno, J.; Nebra, N. *Chem.—Eur. J.* **2007**, *13*, 6590–6594.
- (35) Díaz-Álvarez, A. E.; Crochet, P.; Zablocka, M.; Duhayon, C.; Cadierno, V.; Majoral, J.-P. *Eur. J. Inorg. Chem.* **2008**, 786–791.
- (36) Cadierno, V.; Crochet, P.; Francos, J.; García-Garrido, S. E.; Gimeno, J.; Nebra, N. *Green Chem.* **2009**, *11*, 1992–2000.
- (37) Cadierno, V.; Francos, J.; Gimeno, J. *Green Chem.* **2010**, *12*, 135–142.
- (38) Cadierno, V.; Francos, J.; Gimeno, J. *Chem. Commun.* **2010**, *46*, 4175–4177.
- (39) Díez, J.; Gimeno, J.; Merino, I.; Rubio, E.; Suárez, F. J. *Inorg. Chem.* **2011**, *50*, 4868–4881.
- (40) Bellarosa, L.; Díez, J.; Gimeno, J.; Lledós, A.; Suárez, F. J.; Ujaque, G.; Vicent, C. *Chem.—Eur. J.* **2012**, *18*, 7749–7765.
- (41) Noyori, R.; Hashiguchi, S. *Acc. Chem. Res.* **1997**, *30*, 97–102.
- (42) Porri, L.; Gallazzi, M. C.; Colombo, A.; Allegra, G. *Tetrahedron Lett.* **1965**, *47*, 4187–4189.
- (43) Salzer, A.; Bauer, A.; Podewils, F. In *Synthetic Methods of Organometallic and Inorganic Chemistry*; Herrmann, W. A., Ed.; Thieme Verlag: Stuttgart, Germany, 2000; Vol. 9, p 36.
- (44) Salzer, A.; Bauer, A.; Geyser, S.; Podewils, F.; Turpin, G. C.; Ernst, R. D. *Inorg. Synth.* **2004**, *34*, 59–65.
- (45) Bennett, M. A.; Smith, A. K. *J. Chem. Soc., Dalton Trans.* **1974**, 233–241.
- (46) Bennett, M. A.; Huang, T. N.; Matheson, T. W.; Smith, A. K. *Inorg. Synth.* **1982**, *21*, 74–78.
- (47) Çetinkaya, B.; Özdemir, I.; Bruneau, C.; Dixneuf, P. H. *Eur. J. Inorg. Chem.* **2000**, 29–32.
- (48) Vock, C. A.; Sclaro, C.; Phillips, A. D.; Scopelliti, R.; Sava, G.; Dyson, P. J. *J. Med. Chem.* **2006**, *49*, 5552–5561.
- (49) *Collect, data collection software*; Bruker AXS: Delft, The Netherlands, 2004.
- (50) Otwinowski, Z.; Minor, W. *Methods Enzymol.* **1997**, *276*, 307–326.
- (51) Blessing, R. H. *Acta Crystallogr.* **1995**, *A51*, 3–58.
- (52) *CrysAlis^{Pro} CCD, CrysAlis^{Pro} RED*; Oxford Diffraction Ltd.: Abingdon, Oxfordshire, U.K., 2008.
- (53) WINGX; Farrugia, L. J. *J. Appl. Crystallogr.* **1999**, *32*, 837–838.
- (54) Beurskens, P. T.; Admiraal, G.; Beurskens, G.; Bosman, W. P.; García-Granda, S.; Gould, R. O.; Smits, J. M. M.; Smykalla, C. *The DIRDIF Program System*; Technical Report of the Crystallographic Laboratory; University of Nijmegen: Nijmegen, The Netherlands, 1999.
- (55) SIR-92; Altomare, A.; Casciaro, G.; Giacovazzo, C.; Guàrdi, A. *J. Appl. Crystallogr.* **1993**, *26*, 343–350.
- (56) Sheldrick, G. M. *SHELXL97, Program for the Refinement of Crystal Structures*; University of Göttingen: Göttingen, Germany, 1997.
- (57) *Tables for X-Ray Crystallography*; Kynoch Press: Birmingham, U.K., 1974; Vol. IV (present distributor: Kluwer Academic Publishers; Dordrecht, The Netherlands).
- (58) PARST; Nardelli, M. *Comput. Chem.* **1983**, *7*, 95–98.
- (59) Spek, A. L. *PLATON: A Multipurpose Crystallographic Tool*; University of Utrecht: Utrecht, The Netherlands, 2007.
- (60) Becke, A. D. *J. Chem. Phys.* **1993**, *98*, 1372–1377.
- (61) Becke, A. D. *J. Chem. Phys.* **1993**, *98*, 5648–5652.
- (62) Lee, C.; Parr, R. G.; Yang, W. *Phys. Rev. B* **1988**, *37*, 785–789.
- (63) Stephens, P. J.; Devlin, J. F.; Chabalowski, C. F.; Frisch, M. J. *J. Phys. Chem.* **1994**, *98*, 11623–11627.
- (64) Frisch, M. J.; Trucks, G. W.; Schlegel, H. B.; Scuseria, G. E.; Robb, M.; Cheeseman, J. R.; Montgomery, J. A.; Vreven, J. A.; Kudin, K. N.; Burant, J. C.; Millam, J. M.; Iyengar, S. S.; Tomasi, J.; Barone, V.; Mennucci, B.; Cossi, M.; Scalmani, G.; Rega, N.; Petersson, G. A.; Nakatsuji, H.; Hada, M.; Ehara, M.; Toyota, K.; Fukuda, R.; Hasegawa, J.; Ishida, M.; Nakajima, T.; Honda, Y.; Kitao, O.; Nakai, H.; Klene, M.; Li, X.; Knox, J. E.; Hratchian, H. P.; Cross, J. B.; Adamo, C.; Jaramillo, J.; Gomperts, R.; Stratmann, R. E.; Yazyev, O.; Austin, A. J.; Cammi, R.; Pomelli, C.; Ochterski, J. W.; Ayala, P. Y.; Morokuma, K.; Voth, G. A.; Salvador, P.; Dannenberg, J. J.; Zakrzewski, V. G.; Dapprich, S.; Daniels, A. D.; Strain, M. C.; Farkas, O.; Malick, D. K.; Rabuck, A. D.; Raghavachari, K.; Foresman, J. B.; Ortiz, J. V.; Cui, Q.; Baboul, A. G.; Clifford, S.; Cioslowski, J.; Stefanov, B. B.; Liu, G.; Liashenko, A.; Piskorz, P.; Komaromi, I.; Martin, R. L.; Fox, D. J.; Keith, T.; Al-Laham, M. A.; Peng, C. Y.; Nanayakkara, A.; Challacombe, M.; Gill, P. M. W.; Johnson, B.; Chen, W.; Wong, M. W.; Gonzalez, C.; Pople, J. A. *Gaussian 03, Revision C.02*; Gaussian, Inc.: Pittsburgh, PA, 2004.
- (65) Zhao, Y.; Truhlar, D. G. *Theor. Chem. Acc.* **2008**, *120*, 215–241.
- (66) Frisch, M. J.; Trucks, G. W.; Schlegel, H. B.; Scuseria, G. E.; Robb, M. A.; Cheeseman, J. R.; Scalmani, G.; Barone, V.; Mennucci, B.; Petersson, G. A.; Nakatsuji, H.; Caricato, M.; Li, X.; Hratchian, H. P.; Izmaylov, A. F.; Bloino, J.; Zheng, G.; Sonnenberg, L.; Hada, M.; Ehara, M.; Toyota, K.; Fukuda, R.; Hasegawa, J.; Ishida, M.; Nakajima, T.; Honda, Y.; Kitao, O.; Nakai, H.; Vreven, T.; Montgomery, J. A., Jr.; Peralta, J. E.; Ogliaro, F.; Bearpark, M.; Heyd, J. J.; Brothers, E.; Kudin, K. N.; Staroverov, V. N.; Kobayashi, R.; Normand, J.; Raghavachari, K.; Rendell, A.; Burant, J. C.; Iyengar, S. S.; Tomasi, J.; Cossi, M.; Rega, N.; Millam, J. M.; Klene, M.; Knox, J. E.; Cross, J. B.; Bakken, V.; Adamo, C.; Jaramillo, J.; Gomperts, R.; Stratmann, R. E.; Yazyev, O.; Austin, A. J.

Cammi, R.; Pomelli, C.; Ochterski, J. W.; Martin, R. L.; Morokuma, K.; Zakrzewski, V. G.; Voth, G. A.; Salvador, P.; Dannenberg, J. J.; Dapprich, S.; Daniels, A. D.; Farkas, O.; Foresman, J. B.; Ortiz, J. V.; Cioslowski, J.; Fox, D. J. *Gaussian 09*, Revision A.1; Gaussian, Inc.: Wallingford, CT, 2009.

- (67) Hay, P. J.; Wadt, W. R. J. *Chem. Phys.* **1985**, *82*, 270–283.
- (68) Ehlers, A. W.; Boehme, M.; Dapprich, S.; Gobbi, A.; Hoellwarth, A.; Jonas, V.; Koehler, K. F.; Stegmann, R.; Veldkamp, A.; Frenking, G. *Chem. Phys. Lett.* **1993**, *208*, 111–114.
- (69) Klamt, A.; Schüürmann, G. *J. Chem. Soc., Perkin. Trans.* **1993**, *2*, 799–805.
- (70) Andzelm, J.; Kölmel, C.; Klamt, A. *J. Chem. Phys.* **1995**, *103*, 9312–9320.
- (71) Barone, V.; Cossi, M. *J. Phys. Chem. A* **1998**, *102*, 1995–2001.
- (72) Cossi, M.; Rega, N.; Scalmani, G.; Barone, V. *J. Comput. Chem.* **2003**, *24*, 669–681.
- (73) Hehre, W. J.; Radom, L.; Schleyer, P. v. R.; Pople, J. A. *Ab Initio Molecular Orbital Theory*; Wiley: New York, 1986.
- (74) Chen, P. *Angew. Chem., Int. Ed.* **2003**, *42*, 2832–2847.
- (75) Takats, Z.; Nanita, S. C.; Cooks, R. G. *Angew. Chem., Int. Ed.* **2003**, *42*, 3521–3523.
- (76) Santos, L. S.; Metzger, J. O. *Angew. Chem., Int. Ed.* **2006**, *45*, 977–981.
- (77) Guo, H.; Qian, R.; Liao, Y.; Ma, S.; Guo, Y. *J. Am. Chem. Soc.* **2005**, *127*, 13060–13064.
- (78) Toerien, J. G.; van Rooyen, P. H. *J. Chem. Soc., Dalton Trans.* **1991**, 1563–1568.
- (79) Steed, J. W.; Tocher, D. A. *J. Chem. Soc., Dalton Trans.* **1992**, 2765–2773.
- (80) Jones, C. J.; McCleverty, J. A.; Rothin, A. S. *J. Chem. Soc., Dalton Trans.* **1986**, 109–111.
- (81) García, M. P.; Portilla, A.; Oro, L. A.; Foces-Foces, C.; Cano, F. H. *J. Organomet. Chem.* **1987**, *322*, 111–120.
- (82) For a general review on the coordination chemistry and catalytic applications of complex **1**, see: Cadierno, V.; Crochet, P.; García-Garrido, S. E.; Gimeno, J. *Curr. Org. Chem.* **2006**, *10*, 165–183.
- (83) The distance and angle values found in **1a** for H···Cl1¹ and N2-H-Cl1¹ of 2.66 Å and 148°, respectively, and in **1b** for H···Cl2¹ and N2-H···Cl2¹ of 2.46 Å, and 158°, respectively, suggest the presence of an intermolecular weak hydrogen interaction.
- (84) The analogous ruthenium(II) pyrazole-precatalysts also show a lower catalytic activity (see ref 40).
- (85) Complex **1a** is also active at 35 °C (60 min; 99%).
- (86) It is interesting to note that the catalyst is scarcely soluble in water, the reaction proceeding in a biphasic manner.
- (87) Activity probably being dependent on the different miscibility of the alcohols in water.
- (88) Tissandier, M. D.; Cowen, K. A.; Feng, W. Y.; Gundlach, E.; Cohen, M. H.; Earhart, A. D.; Coe, J. V.; Tuttle, T. R. *J. Phys. Chem. A* **1998**, *102*, 7787–7794.
- (89) Pliego, J. R., Jr.; Riveros, J. M. *Phys. Chem. Chem. Phys.* **2002**, *4*, 1622–1627.
- (90) Kovács, G.; Rossin, A.; Gonsalvi, L.; Lledós, A.; Peruzzini, M. *Organometallics* **2010**, *29*, 5121–5131.
- (91) In the cis-hydroxo route of the benzimidazole complex the acrolein hydrogenation is stepwise, hydride transfer preceding proton transfer. However, the two transition states located have very similar energies and are separated by a very shallow minimum (see ref 92).
- (92) The asynchronicity in ketone hydrogenation by bifunctional ruthenium catalysts has been recently analyzed: Chen, Y.; Tang, Y.; Lei, M. *Dalton Trans.* **2009**, 2359–2364.
- (93) Described as the energetic span of the catalytic cycle: Kozuch, S.; Martin, J. M. L. *ChemPhysChem* **2011**, *12*, 1413–1418.
- (94) Stabilization of the transition state of asymmetric transfer hydrogenation of ketones by hydrogen bonding has been reported: Wu, X.; Liu, J.; Di Tommaso, D.; Iggo, J. A.; Catlow, C. R. A.; Bacsá, J.; Xiao, J. *Chem.—Eur. J.* **2008**, *14*, 7699–7715.